Arabian Journal for Science and Engineering
https://doi.org/10.1007/s13369-022-07312-4

RESEARCH ARTICLE-CHEMICAL ENGINEERING

Structural Properties and Degradation Efficiency Photocatalyst-based Composite Titanium Dioxide/Activated Carbon by Charge Trap System for Groundwater Reach Phenol Treatment

Bidayatul Armynah[1] · Sitti Hajar[1] · Roni Rahmat[1] · Ahmad Nurul Fahri[1] · Paulus Lobo Gareso[1] · Heryanto Heryanto[1] · Dahlang Tahir[1]

Received: 14 May 2022 / Accepted: 20 September 2022

Abstract
High recombination of the photoexcited electron–hole pairs leading to a drop in the photocatalytic performance. The pore of activated carbon (AC) can be act as a trap of the charge of electron/hole (e/h) which can suppress recombination. The objective in this study maximizing function of the pore of AC for create composite combine with TiO_2 that can act in visible light. In the pore, the reaction occurs between the charge and the H_2O or O_2 produces OH^* radicals. These radicals entering the chemical site of pollution to break up the bonding with the final product are harmless. The prepared composite TiO_2/activated carbon (TAC) by wet impregnation method were characterized by X-ray diffraction, Fourier-transform infrared, and ultraviolet–visible spectroscopy. Composite TAC with ratio 0.5:1.5, 1:1, 1.5:0.5 shows degradation 94.06%, 94.91%, and 88.98%, respectively, for only 45 min irradiation, indicated that the pore successfully suppressing recombination of the charge. We have performed good efficiency for five adsorption–desorption cycles of TAC. The TAC 1:1 ratio shows the best photocatalyst performance which degraded 94.91% for 45 min irradiation. The composite TAC shows high potential in suppressing recombination of charge, means that, effective and efficient ground wastewater treatment materials in future for improvement human access to the clean water.

Keywords Photodegradation · Composite titanium dioxide/activated carbon · Bandgap · Kinetic study · Fourier-transform infrared

1 Introduction

Raizada et al. [1] and Zhang et al. [2] reported that the development of the textile industry has a significant impact on environmental pollution and human health. Gaya et al. [3] reported that the waste produced from the textile industry consists of organic dyes, inorganic, acids, and heavy metals. Theerthagiri et al. [4] reported that one of these products is dye waste, generally non-biodegradable organic compound, and causes environmental pollution, especially the aquatic environment. Alinsafi et al. [5] reported that a more effective and developed system is the photodegradation method using semiconductor materials. Fayazi et al. [6] reported that the photodegradation process using energy derived from light (sunlight or UV lamps) to activate the catalysis process on the surface of the semiconductor material. This process produces hydroxyl radicals OH^* to degrade organic pollutants and dyes. Several studies reported that TiO_2 is a promising photocatalyst for reducing waste due to its photostability, low energy consumption, low cost, and non-toxicity [7–9]. The TiO_2 bandgap, which only absorbs UV sunlight, requires supporting materials to increase photocatalytic activity [10, 11]. Khalyavka et al. [12] and Ren et al. [13] reported that the photocatalytic activity of TiO_2 can be increasing by modifying the structure, surface area, and particle size by adding dopant ions such as carbon. Matos et al. [14] said that carbon-doped TiO_2 has a higher photocatalytic activity than without doping.

It has been well reported by several research groups that the incorporation carbon atoms into TiO_2 lattice is an efficient method for improving the adsorption capacities in photocatalyst system [15]. It has been used for expanding the photon absorption to the visible region [16] and for increasing the

✉ Dahlang Tahir
dtahir@fmipa.unhas.ac.id

[1] Departement of Physic, Hasanuddin University, Makassar 90245, Indonesia

Published online: 03 October 2022

TiO_2 conductivity, which can help the charge transfer from the bulk to the surface TiO_2 consequently the oxidation reactions at the surface of TiO_2 increases [17].

Some studies reported successfully designed photocatalyst working at visible light using carbon-doped titania at low temperature, combination carbon-titania [13], and the atoms carbon incorporated into TiO_2 framework. For activated carbon (AC) combine with TiO_2 for photocatalyst is used to find possibilities the pore of AC in increasing efficiency of TiO_2. In our previous study, our group reported the materials for photocatalyst which used a combination some material with activated carbon (AC): Fe_3O_4–AC [18], Fe–AC [19], AC plays dual roles of capable electron-acceptor and charge trap for avoiding recombination, which keeps the charge react with H_2O or O_2 to increase efficiency photocatalyst TiO_2-based. The pore of carbon-based materials also used the pore in various application including photocatalyst and energy storage.

Carbon-based materials for supercapacitors application by electrochemical energy storage through reversible ion adsorption by the complex structure of the porous carbons as electrodes. The supercapacitors for the same average pore size with ordered structure has higher capacitance compared with that than the disordered structure and a broader pore size distribution. They reported that the number of ions adsorbed in the ordered pore carbon shows larger quantities compared with that of disordered pore carbon [20].

Reference. [21] was reported that the space confinement in nanopores used in the collision frequency which are increased linearly with increasing pore size up to 3 nm. The pore is also efficient reaction space used for reduction of oxygen.

The existence ionic states of As and surface charge states of hydrous cerium oxides (HCO) was reported by Li et al. [22]. The surface of HCO nanoparticles was negatively charged with no existed repulsive force between surface HCO nanoparticle surface. For high pH (> 9.2), the surface negatively charged HCO nanoparticle will start to have the coulomb repulsive force. The electric repulsion increased with the increasing the pH solution but the As ion removal continued to decrease [22].

The carbon as a nonmetallic element is used to substitute lattice oxygen anions of Ti cations to create energy levels as an active site in the bandgap. This energy level is acted as an electron trapper to suppress indirect recombination of charge (electrons and holes). It can be shifts to lower energy of TiO_2 optical absorption edge for extend the photoactive region in the visible light. For large surface area could provide the more active sites at the surface and in photocatalytic centers for suppressing recombination of charge (e/h) lead to higher absorption of organic pollutants consequently higher photocatalytic efficiency. For higher crystallinity degree and low surface defects will facilitating charge carrier transform and hindered charge (e/h) recombination which beneficial for increasing photocatalytic efficiency [23].

The surface function of activated carbon (AC) plays an essential role in the photoactivity of TiO_2 as a support material to adsorb many organic pollutants. Elshaghi et al. [24] was reported that the AC has a good surface area and a porous structure to be used as an absorbent. The nature of AC can help the absorption process in catalytic activity. For our knowledge, few reported in references for using pore of AC as a magnetic trap of the charge (e/h). In our previous study showed that the pore of AC could be used as a trapped charge (e/h) and successfully increase photocatalyst performance [18, 19, 25]. In the pore, the reaction between the charge and the H_2O or O_2 produces OH^* radicals. These radicals entering the chemical site of pollution/phenol to break up the bonding with the final product are harmless. Hence, in this study, we synthesized TAC by wet impregnation method with the weight ratio between TiO_2 and AC are 0.5:1.5, 1:1, and 1.5:0.5. We are continue characterizing the TAC by X-ray diffraction (XRD) for determining the structural properties, Fourier-transform infrared (FTIR) for bonding characteristics, scanning electron microscope (SEM) image for surface functional (pore), and kinetic study of composite TiO_2/AC for various ratio between TiO_2 and AC using the visible light and the ability of these materials by the process photodegradation using several theoretical methods.

2 Materials and Method

2.1 Materials

TiO_2 (Merck), activated carbon (AC) (supplied by PT. Cahaya Indo Abadi Indonesia with sizing an average diameter < 10 μm, purity > 95%, surface area > 240 m/g), Ethanol (C_2H_5OH) (Merck), Methylene Blue (MB) (Merck) and Aquadest.

2.2 Synthesis TiO_2/AC

TiO_2 and activated carbon were synthesized by wet impregnation method with the weight ratio between TiO_2 and AC are 0.5:1.5, 1:1, and 1.5:0.5 to form TAC. The TAC is added with 30 mL ethanol then stirring by magnetic stirrer for the constant speed of 200 rpm at the temperature 60 °C until form gel, and then calcined by using furnace at 100 °C for 3 h to form powder.

2.3 Characterization

Samples characterized using X-ray diffraction (XRD) (Shimadzu 700) with CuKα ($\lambda = 1.5405$ Å $= 0.154$ nm) at an angle of range $20° \leq 2\theta \leq 70°$ operating at 30 kV and 10 mA)

to determine the structural properties. Fourier-transform infrared (FTIR) to determine the bonding characteristics of the sample and UV–Vis spectroscopy (Shimadzu UV–Vis Spectrophotometers UV-1800) determines the bandgap and the absorption properties.

3 Result and Discussion

Figure 1a shows XRD spectra of TiO_2/AC composites for various concentration ratio. The diffraction spectra from the individual of TiO_2 and carbon from AC. The TiO_2 diffraction peaks at 2θ: 25.20°, 32.60° 33.24°, 35.90°, 47.98°, 53.63°, 53.89°, and 64.48° (JCPDS: 01-088-1172) corresponding to the crystalline phase (101), (111), (203), (101), (212), (105), (211), and (310), respectively (Zhu et al. [26]). The activated carbon diffraction peaks at 2θ: 26.49°, 26.58°, 29.33°, 30.91°, 42.98°, and 54.51° (JCPDS: 00-050-0926) corresponding to the crystalline phase (002), (103), (113), (122), (100), and (103), respectively (Brown et al. [27]). The XRD spectra show the diffraction intensity decreases and the diffraction peak is slightly shifted due to the addition of activated carbon. TiO_2/AC shows that the synthesis product is still in the anatase TiO_2 phase, where the anatase phase has a high activation, a larger surface area and a smaller particle size.

The crystallite size calculated using the Debye–Scherrer equation as follows Zhu et al. [26]:

$$d = \frac{0.9 \cdot \lambda}{\beta \cos\theta} \tag{1}$$

where d is the crystal size, λ is the X-ray wavelength (λ = 1.5406 Å), β is the full width at half maximum (FWHM) and θ is the X-ray diffraction angle at the highest peak (radians). The mean crystallite size was found 7.98 nm, 8.31 nm, and 8.19 nm, respectively, for TAC 1:1, 0.5:1.5, and 1.5:0.5. It is appearing that the lowest crystallite size is for TAC 1:1 may be due to the stable match electronic structure between TiO_2 and carbon from AC [28–32]. Based on our previous research group, the particle size determining from the quantitative analysis of scanning electron microscope (SEM) or transmission electron microscope (TEM) image showed that generally two or three times higher than that of crystallite size for CuO/Carbon [25], Co/Fe_2O_3/AC [33], and Carbon-lignin/Zinc Oxide [34]. This proof for the results in this study the particle size is higher than 20 nm.

Pambudi et al. [35] was reported that the FTIR analysis in determining the functional groups of materials and for composites TAC in this study, the wave number in the range 500–4000 cm^{-1} shown in Fig. 1b. For the wave numbers 538 cm^{-1} and 906 cm^{-1} indicated the presence of aromatic rings in the form of C=C–C bonds bonding with Ti–O caused by tensile vibrations as reported by Suganthi et al. [36] and Ulum et al. [34]. Bagheri et al. [37] was reported for the wave numbers 677 cm^{-1} and 1446 cm^{-1} there are C–Ti–O and O–Ti–O bonds, respectively, which indicated the presence TiO_2 in TAC [38]. Ulum et al. [34] in the 1826 cm^{-1} wave there is a C=C–C bond. Rauf et al. [39] for the Ti^{2+} probably bonding with –OH bond appears at the 2343 cm^{-1} wave number which causes the vibration of the hydroxyl or water molecule bonds adsorbed on the activated carbon similar reported by Eshaghi et al. [24] in the 3844 cm^{-1} for OH^- bond from the absorbed water molecule as reported in the wave number 3649–3844 cm^{-1} by Rizkayanti et al. [40]. Samsudin et al. [41] for the 2540 cm^{-1} wave number there is a Ti–OH bond. Yu et al. [42] and Yang et al. [43] for the wave number 2910–3041 cm^{-1} there are –OH bonds. Munguti et al. [44] reported for a strain vibration from the C–H bond in the 3421 cm^{-1} due to the absorption of the alkane groups. Brown et al. [27] reported for 3682 cm^{-1} indicated the presence of Ti–OH bonds in the interactions between the carbon atoms.

The intensity of C=C–C and O–H bonds increases with increasing the amount of AC contributed to the change's crystallinity and surface state of TAC [45]. The FTIR spectra show some absorption peaks (C=C–C and O–Ti–O) shifts to higher wave numbers due to the carbon aromatic groups in TAC contributed in increase oxygen vacancies at surface state of the pore [46].

The pore and agglomeration of TAC clearly can be seen in SEM image in Fig. 2. The agglomeration is due to the small size of particles joint together to form big particle and the pore come from the AC shows increase disorder size and shape when the amount of AC decrease from (a) to (c) in composite TAC. For high amount AC (a) shows some of the TiO_2 particle approach to the surface state of the pore and for low amount of AC shows TiO_2 particle start to bind and filled the pore of AC. For same amount of TiO_2 and AC in composite TAC (b) shows the TiO_2 particle tightly bonded at surface state of AC probably due to the oxygen vacancies replaced by C atoms indicated by the pore size increased. For large surface area could provide more active sites at the surface and in photocatalytic centers for suppressing recombination of charge (e/h) lead to higher absorption of organic pollutants consequently boosting photocatalytic efficiency [23]. Lahrar et al. [20] was reported for the same average pore size with ordered structure has higher capacitance (capture ion) compared with that than the disordered structure and a broader pore size distribution. They also reported that the larger quantities ions adsorbed for AC with ordered pore compared with that of disordered pore.

From Fig. 2 also clearly agglomeration occurred, and the shape, the pore size, and particle size distributions are non-uniform which probably leading to increasing oxygen vacancies as reported recently by Zhang et al. [47] and

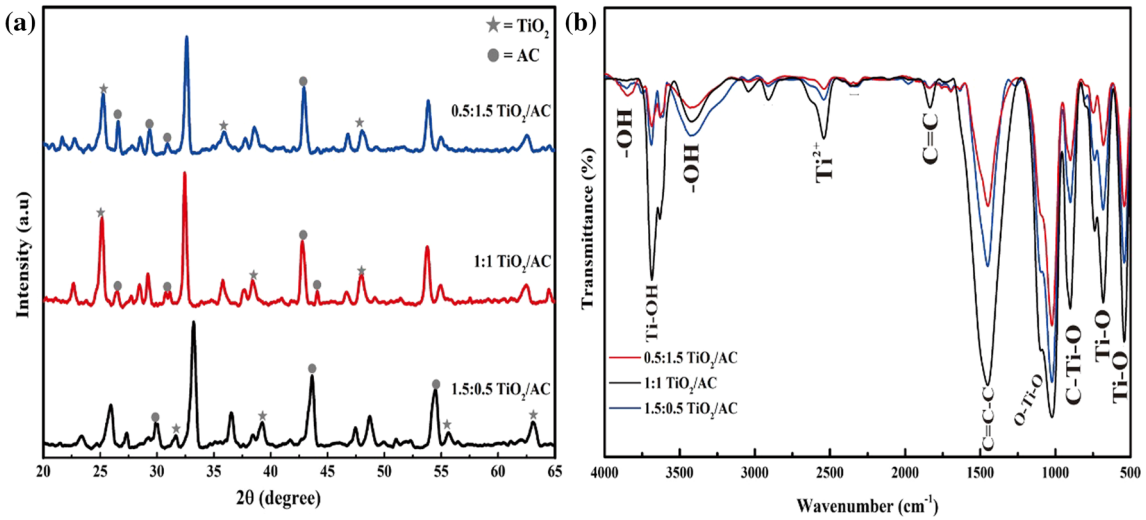

Fig. 1 **a** X-diffraction (XRD) spectra and **b** FTIR spectra for ratio TiO_2/AC: 0.5:1.5, 1:1, and 1.5:0.5

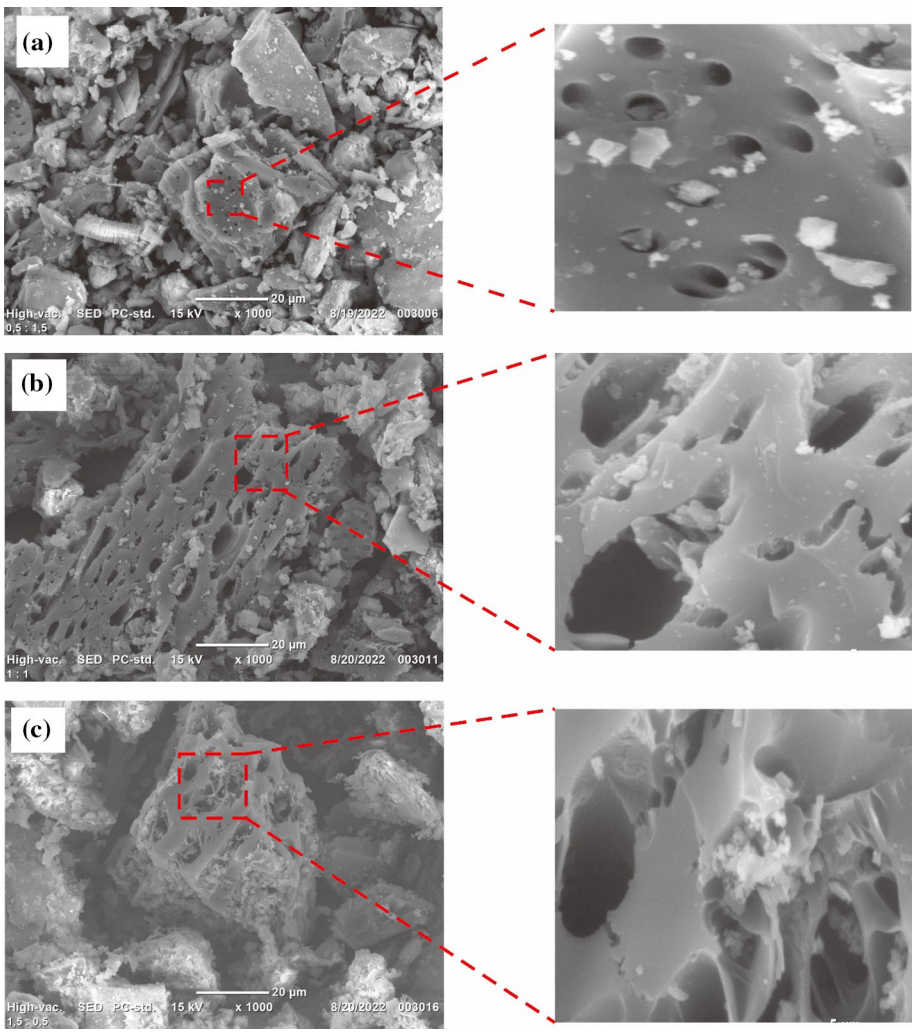

Fig. 2 Scanning electron microscopy (SEM) images of composites TAC for ratio between TiO_2 and AC: **a** 0.5:1.5, **b** 1:1, and **c** 1.5:0.5 for the left side and corresponding zoom in for right side

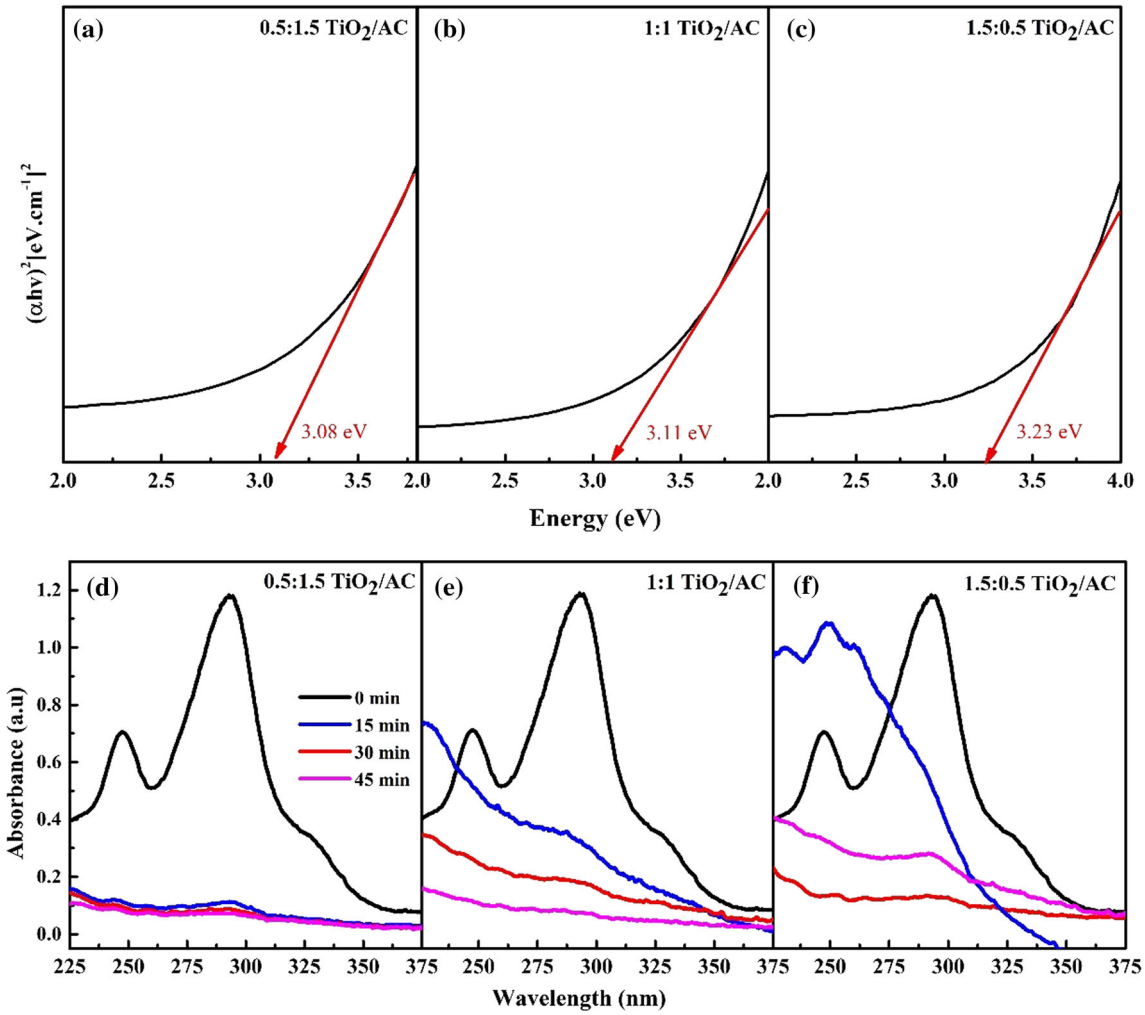

Fig. 3 **a**–**c** Bandgap from the analysis of absorption spectra **d** and **e** the absorbance spectra for TiO_2/AC (TAC) ratio: 0.5:1.5 (left **a** and **d**), 1:1 (middle **b** and **e**), and 1.5:0.5 (right **c** and **f**)

Yakovenko et al. [48]. The charge state from Ti^{+2} at the surface state of the pore changes due to the oxygen vacancy content increase and consequence changes electrical properties and optical bandgap [23]. The oxygen vacancies also contributed for destroy the grain size and increase unit cell parameter as reported by Ref. [49], consequently changes in structure and orientation of the grains size lead to the change porosity, consequently decrease active site for suppressing recombination of charge (e/h). Kozlovskiy et al. [50] was reported that the metal oxide will be influenced to the morphology and electronic properties of the composite TAC due to oxygen vacancies redistribution, consequently affected to the ability in hindered charge (e/h) for increase performance photocatalyst [23].

Bandgap energy is the minimum energy required to excite from the valence band to the conduction band (Munguti et al. [44]). Figure 3a–c shows the bandgap of composite TAC obtained from the absorbance spectrum by applying the Tauc's plot method. This method is determining the optical bandgap by taking the linear graph in the figure relationship between photon energy on the x-axis and absorption coefficient $(\alpha hv)^2$ on the y-axis. The bandgap of TAC composite increases with increasing the amount of TiO_2 in TAC composite even the AC higher bandgap than the TiO_2 may be due to the deficiency oxygen atom from the AC [51].

Figure 3d–f shows the absorbance spectra from the UV–Vis spectroscopy for TAC composite in the methylene blue solvent during irradiation of visible light for every 15 min. The absorbance values for methylene blue are in the range of 200–400 nm wavelength. The absorbance decreases with increasing irradiation time. The maximum absorbance was observed for methylene blue at the wavelength of 293 nm.

Figure 4a shows the degradation of TAC during irradiation time up to 45 min. Ulum et al. [34] reported the calculation

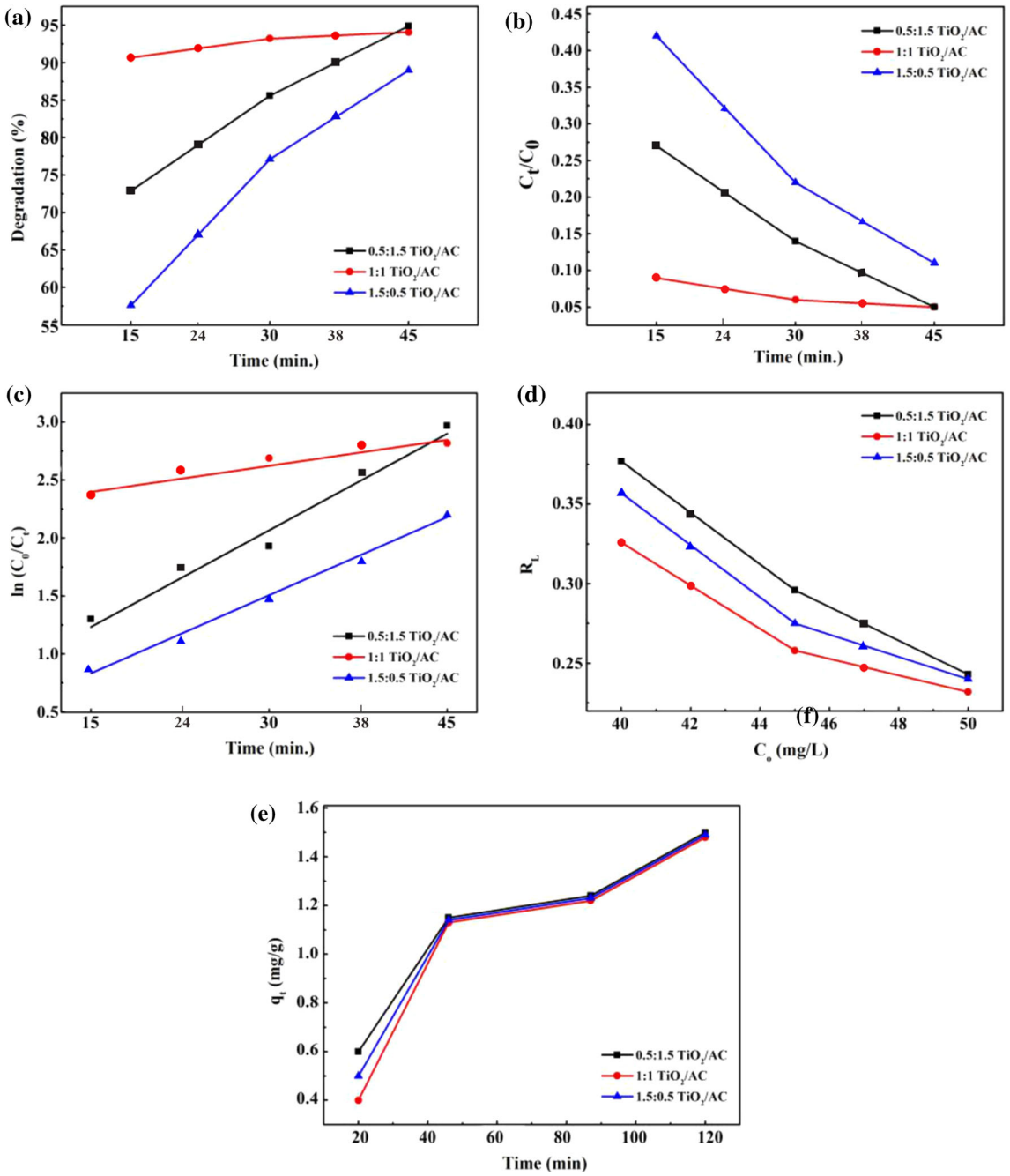

Fig. 4 **a** Photodegradation efficiency, **b** the performance of the photocatalyst, **c** the kinetic rate, **d** equilibrium parameter (R_L), and **e** the adsorption capacity of the TAC Composite for ratio TiO_2/AC: 0.5:1.5, 1:1, and 1.5:0.5

of the degradation by:

$$\%D = \left(\frac{C_0 - C_t}{C_0}\right) \times 100\% \tag{2}$$

where % D is the degradation percentage, C_0 is the initial absorbance (before irradiation), and C_t is the absorbance during irradiation t time. For TAC composite 0.5:1.5, 1:1, 1.5:0.5 shows maximum degradation for 45 min irradiation is 94.06%, 94.91%, and 88.98%, respectively. We have included in Table 1 the previous reported references using various type of carbon: activated carbon, carbon nanotubes, and multi-wall carbon nanotubes (MWCNT) from the different synthesized methods for comparison in this study. From Table 1, clearly the effectiveness composite TiO_2/AC (TAC) synthesized by wet impregnation only 45 min irradiation to reach degradation 94.06%. The TAC synthesized by sol–gel

Table 1 The TiO_2/activated carbon (TAC) in this study synthesized by wet impregnation, and we have included the composite TiO_2/various type of carbon from the previous published reference for comparison

Material	Method	Pollutant	Efficiency	Refs.
TiO_2/activated carbon	Sol–gel synthetic method	Tetracycline (50 mg L^{-1})	100% in 150 min	[52]
TiO_2/activated carbon	wet impregnation	Methylene Blue (50 mg L^{-1})	94.05% in 45 min	Present study
TiO_2@C	Heat treatment and solid-state method	Tetracycline (20 mg L^{-1})	97.12% in 30 min	[53]
Carbon-TiO_2 nanotubes	Electrospinning and heat treatment method	Unsymmetrical dimethylhydrazine (50 mg L^{-1})	90% in 2 h	[54]
TiO_2/amorphous carbon/carbon nanotube film	Simple atomization spray method	Rhodamine B	91.29% in 120 min	[55]
Multi-wall carbon nanotube (MWCNT)/titanium dioxide nanocomposites	Low-temperature sol–gel method and a simple evaporation and drying process	Bismarck brown R dye (100 mL; 5×10^{-5} M)	82.7% in 90 min	[56]
TiO_2/Multi-wall carbon nanotube	Sol–gel and ultrasound waves method	Methylene blue (10 ppm)	61.6% in 70 min	[57]

methods was reported by Ref. [52] need 150 min for degraded tetracycline 100%, but Ref. [53] was reported synthesized TiO_2/carbon by heat treatment and solid-state method shows more shorter which need only 30 min.

Figure 4b and c shows the kinetic rate of the TAC composite for the photodegradation of methylene blue, in Fig. 4b the performance during irradiation causes the concentration of contaminants decrease sharply for TAC 1:1. Figure 4c shows the kinetic rate of TAC composite (Rauf et al. [39]) by ln (C_0/C_t) versus irradiation time with k is kinetic rate constant calculated as follows:

$$\ln\frac{C_0}{C_t} = k \cdot t \tag{3}$$

where C_0 is the initial absorbance (before being irradiated), C_t is the absorbance after the photocatalyst process at the time t, t is the time of the photodegradation process and R^2 is the correlation coefficient.

The uptake at equilibrium, q_e (mg g^{-1}), was calculated by the following equation:

$$q_e = \frac{(C_{01} - C_e)V}{W} \tag{4}$$

where C_{01} is the initial concentration of solution (in this study, 50 mg L^{-1}), C_e (mg L^{-1}) is the equilibrium concentration of solution, V is the volume of solution (in this study is 0.03 L), and W is the weight of activated carbon.

The absorption capacity at time t, q_t (mg g^{-1}) as shown in Fig. 4, was calculated using the following equation:

$$q_t = \frac{(C_{01} - C_t)V}{W} \tag{5}$$

where C_t (mg L^{-1}) is the equilibrium concentration of solution at time t (min).

Figure. 4e shows that the adsorption capacity is increasing for TAC 0.5:1.5, this is due to the higher carbon concentration where the pore use as a trap in adsorption process.

Cheng et al. [58] was reported for pseudo-first order and pseudo-second order kinetic models by choose the best fitted model to the correlation coefficient (R^2) and the standard deviation (Δq) as follow:

$$\Delta q = 100\sqrt{\frac{1}{N-1}\sum_{i=1}^{i=N}\left[\frac{q_{t,\exp} - q_{t,cal}}{q_{t,\exp}}\right]^2} \tag{6}$$

The (R^2) and Δq values for adsorption kinetic models were calculated where $q_{t,\mathrm{cal}}$ means calculated and $q_{t,\exp}$ means experiment adsorption values. The pseudo-first order model:

$$\mathrm{Ln}(q_e - q_t) = \ln q_e - k_1 t \tag{7}$$

and the pseudo-second order model:

$$\frac{t}{q_t} = \frac{1}{K_2 q_e^2} + \frac{t}{q_e} \tag{8}$$

Benedetto et al. [59] reported diffusion model developed by Weber and Morris for the adsorption mechanism with the intraparticle:

$$q_t = K_{\mathrm{id}}\sqrt{t} + A \tag{9}$$

where K_{id} is diffusion rate constant of the intraparticle (mg g^{-1} $min^{-0.5}$) and A (mg g^{-1}) is a constant proportional

Table 2 Kinetic rate constant determined by Eq. (3) for k, pseudo-first order for k_1, and pseudo-second order for k_2, and correlation coefficient (R^2) of TAC composites

TAC	k (min^{-1})	k_1 (min^{-1})	k_2 (min^{-1})	R^2
0.5:1.5	0.062	0.025	0.082	0.90918
1:1	0.066	0.031	0.075	0.96061
1.5:0.5	0.048	0.019	0.063	0.99558

of the boundary layer. By plotting q_t versus $t^{1/2}$ will provide the dependency of adsorption on intraparticle diffusion. For only intraparticle diffusion is affect to the adsorption process, the plot produces a straight line but for additional another phenomena contribution to the adsorption process will multi-linear lines.

For understand the adsorption behavior, the Langmuir and Freundlich isotherms models were the most used to analyze the experimental data.

Langmuir isotherms:

$$\frac{C_e}{q_e} = \frac{1}{K_L q_{max}} + \frac{C_e}{q_{max}} \tag{10}$$

Freundlich isotherms:

$$\mathrm{Ln} q_e = \ln K_f + \frac{1}{n} \ln C_e \tag{11}$$

Fernandez et al. [60] was reported that the characteristics of the Langmuir isotherm in a term of equilibrium parameter (RL) as follows:

$$R_L = \frac{1}{1 + K_L C_0} \tag{12}$$

where K_L is the Langmuir isotherm constant and C_0 is the initial absorbance concentration. The value of R_L indicates the nature of the adsorption: for irreversible the R_L is 0, for favorable the R_L is in between 0 and 1, for linear the R_L is 1, and for unfavorable the R_L is > 1. In this study shows the R_L is in between 0 and 1 indicated the nature of adsorption in favorable as can be seen in Fig. 4d.

Table 2 shows the value of the kinetic rate constant and the correlation coefficient. For the pseudo-second order shows linear dependent with the amount of AC in TAC composite, indicated that the AC play an important role in the proses of adsorption. For another method shows the TAC 1:1 higher than other TAC indicated that the strong atomic bonding and very good matching electronic structure between TiO_2 and carbon [18]. Based on the calculated data, the concentration TAC 1:1 has the highest kinetic rate constant value, this is related to the efficiency of has a smaller crystal size of 7.98 nm. Based on research conducted by Selvi et al. [61] showed that decreasing the crystal size has the potential to increase the specific surface area of the catalyst. This affects the active reaction in increasing the photocatalytic activity.

Figure 5c shows the results of the catalyst being reused 5 times in a row with the best results on TAC composites at a concentration of 1:1 with an irradiation time of 45 min. The catalyst that is used repeatedly in methylene blue dye is used to see the efficiency as reported by Xu et al. [62] The percentage of degradation clearly can still reduce the dye solution, repeated use of the catalyst has decreased the percentage of degradation, due to the loss of catalyst mass during the washing process. This shows the efficiency of the catalyst being reused with a significant reduction. Based on the results, the concentration of 1:1 TAC in cycle 5, has the best degradation with a value 71.24%.

The schematic illustration mechanism of methylene blue degradation using TAC is shown in Fig. 5a and b. The photon from the UV and visible will transfer their energy to the electron at the valence band (VB) of TiO_2 for jump to the conduction band (CB) and remain hole at the VB [28]. For Fig. 5b the electron from CB jump to VB of AC and then receive energy to jump to the CB of AC, this process for suppressing recombination of (e/h). The AC as a nonmetallic element is substituted lattice oxygen for TiO_2 to create active site energy levels in the bandgap which acted as an electron trapper to suppress indirect recombination of charge (e/h). The active site energy levels are contributed for shifting optical absorption edge of TiO_2 to lower energy level for extend to the visible light of the photoactive region. Reference. [23] also was reported that for the small amount of N or Fe ions act as the trap sites for charge (e/h) and inhibit the charge (e/h) recombination will improve drastically the photocatalytic performance. For Fig. 5a shows the pore of AC use as a trap of the charge for reduce recombination [30]. The electron and hole will be trapped in the pore and interact with O_2 and H_2O, respectively, for resulting radical's atoms O_2^- and OH^-. These radicals will be processing degradation by breaking the bond of pollutant (indicated by scissor in Fig. 5a) with the final product is H_2O and CO_2 [19].

The AC in composite TiO_2/AC is used to prevent leaching, recovery, and reuse of the composite for photodegradation MB by the process as follows:

$$TiO_2/AC + hv \rightarrow TiO_2/AC\left(e_{CB}^-\right) + TiO_2/AC\left(h_{VB}^+\right) \tag{13}$$

at the valence band:

$$TiO_2/AC\left(h_{VB}^+\right) + H_2O \rightarrow TiO_2/AC + H^+ + OH^{-*} \tag{14}$$

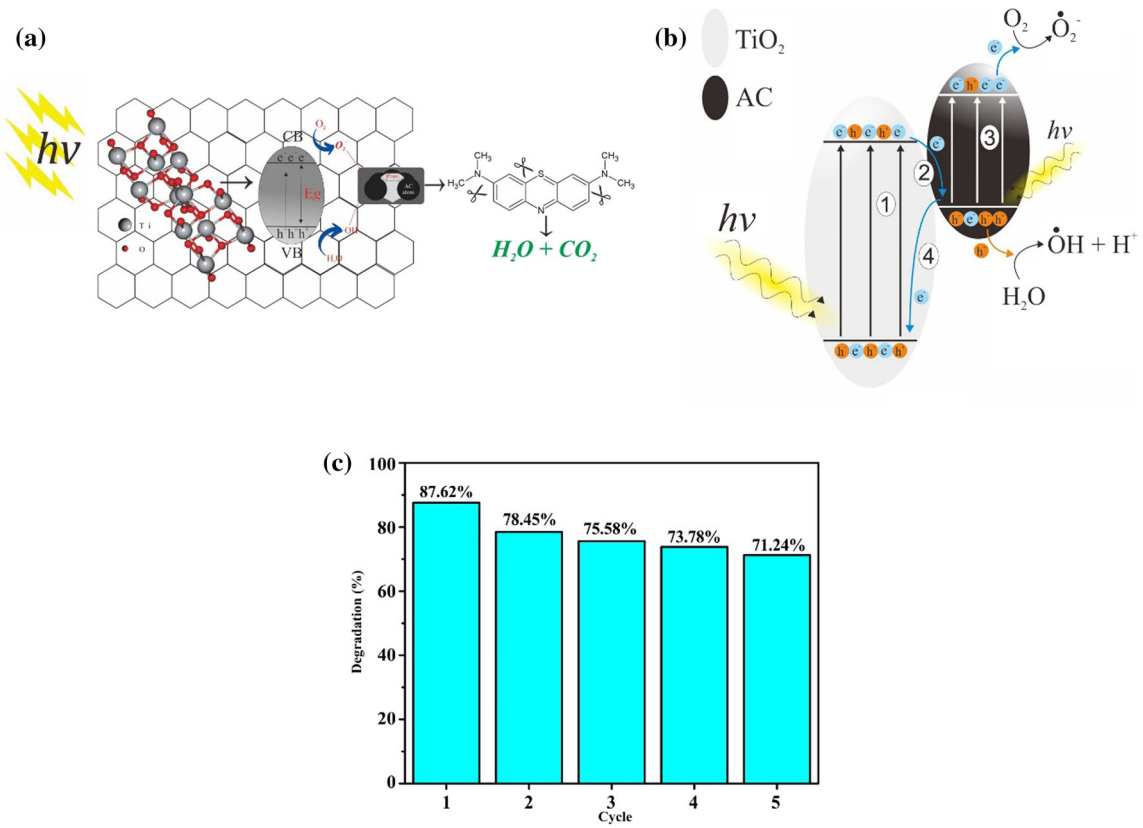

Fig. 5 Methylene blue degradation process **a** the scheme for pore of AC as a trap the charge **b** for Z scheme photocatalyst using TiO_2/AC, and **c** The photocatalyst degradation cycle of TiO_2/AC (TAC) composites 1:1

at the conduction band:

$$TiO_2/AC(e_{CB}^-) + O_2 \rightarrow +TiO_2/AC + O_2^{*-} \quad (15)$$

$$O_2^{*-} + H^+ \rightarrow OOH^* \quad (16)$$

$$O_2^{*-} + H_2O \rightarrow OOH^* + OH^- \quad (17)$$

$$OOH^* + H^+ + TiO_2/AC(e_{CB}^-) \rightarrow H_2O_2 + TiO_2/AC \quad (18)$$

$$OOH^* + H_2O_2 + TiO_2/AC(e_{CB}^-) \rightarrow H_2O_2 + OH^- + TiO_2/AC \quad (19)$$

$$H_2O_2 + TiO_2/AC(e_{CB}^-) \rightarrow OH^* + OH^- + TiO_2/AC \quad (20)$$

$$H_2O_2 + OH^- \rightarrow 2OH^* + OH^- \quad (21)$$

$$H_2O_2 + hv \rightarrow 2OH^* \quad (22)$$

$$OH^* + MB \rightarrow H_2O + CO_2 \quad (23)$$

4 Conclusion

The FTIR showed intensity of C=C–C and O–H bonds increases with increasing the amount of AC play important role to the change's crystallinity and surface state of TAC. The AC was substituted lattice oxygen of TiO_2 to create active site in the bandgap to suppress indirect recombination of charge (e/h) which contributed for shifting optical absorption edge of TAC for extend to the visible light of the photoactive region. The C=C–C and O–Ti–O absorption peaks shifts to higher wave numbers due to the oxygen vacancies increase at the surface state of the pore.

The SEM clearly showed pore and agglomeration of TAC indicated by increases disorder size and shape when the amount of AC decreasing in composite TAC. For high amount AC the TiO_2 particle approach to the surface state of the pore and tightly bonded with AC probably due to the oxygen vacancies replaced by C atoms indicated by the pore size increased. We found that the best samples in this study is for ratio composite TAC is 1:1, indicated by the best photocatalyst performance which was supported by the analysis XRD spectra showed the smaller crystal size (7.98 nm). The pore of AC is a trap of the charge (electron and hole) for reduce recombination indicated by the TAC faster degradation up to

94.05% for only 45 min and can be reused for 5 cycles with efficiency higher than 70%. The TAC in this study as a new composite shows high potentials for effective and efficient wastewater treatment.

Funding Not available.

Declarations

Conflict of interest The authors declared no potential conflict of interest with respect to the research, authorship, and/or publication of this article.

References

1. Raizada, P.; Kumari, J.; Shandilya, P.; Dhiman, R.; Pratap Singh, V.; Singh, P.: Magnetically retrievable Bi_2WO_6/Fe_3O_4 immobilized on graphene sand composite for investigation of photocatalytic mineralization of oxytetracycline and ampicillin. Process Saf. Environ. Prot. **106**, 104–116 (2017). https://doi.org/10.1016/j.psep.2016.12.012
2. Zhang, H.; Huang, H.; Ming, H.; Li, H.; Zhang, L.; Liu, Y.; Kang, Z.: Carbon quantum dots/Ag_3PO_4 complex photocatalysts with enhanced photocatalytic activity and stability under visible light. J. Mater. Chem. **22**, 10501–10506 (2012). https://doi.org/10.1039/C2JM30703K
3. Gaya, U.I.; Abdullah, A.H.: Heterogeneous photocatalytic degradation of organic contaminants over titanium dioxide: a review of fundamentals, progress and problems. J. Photochem. Photobiol. C Photochem. Rev. **9**, 1–12 (2008). https://doi.org/10.1016/j.jphotochemrev.2007.12.003
4. Theerthagiri, J.; Chandrasekaran, S.; Salla, S.; Elakkiya, V.; Senthil, R.A.; Nithyadharseni, P.; Maiyalagan, T.; Micheal, K.; Ayeshamariam, A.; Arasu, M.V.; Al-Dhabi, N.A.; Kim, H.-S.: Recent developments of metal oxide based heterostructures for photocatalytic applications towards environmental remediation. J. Solid State Chem. **267**, 35–52 (2018). https://doi.org/10.1016/j.jssc.2018.08.006
5. Alinsafi, A.; Evenou, F.; Abdulkarim, E.M.; Pons, M.N.; Zahraa, O.; Benhammou, A.; Yaacoubi, A.; Nejmeddine, A.: Treatment of textile industry wastewater by supported photocatalysis. Dyes Pigments **74**, 439–445 (2007). https://doi.org/10.1016/j.dyepig.2006.02.024
6. Fayazi, M.; Taher, M.A.; Afzali, D.; Mostafavi, A.: Enhanced Fenton-like degradation of methylene blue by magnetically activated carbon/hydrogen peroxide with hydroxylamine as Fenton enhancer. J. Mol. Liq. **216**, 781–787 (2016). https://doi.org/10.1016/j.molliq.2016.01.093
7. Tan, J.; Li, Z.; Li, J.; Wu, J.; Yao, X.; Zhang, T.: Graphitic carbon nitride-based materials in activating persulfate for aqueous organic pollutants degradation: a review on materials design and mechanisms. Chemosphere **262**, 127675 (2021). https://doi.org/10.1016/j.chemosphere.2020.127675
8. Lang, X.; Zhao, J.; Chen, X.: Visible-light-induced photoredox catalysis of dye-sensitized titanium dioxide: selective aerobic oxidation of organic sulfides. Angew. Chem. Int. Ed. **55**, 4697–4700 (2016). https://doi.org/10.1002/anie.201600405
9. Sedaghati, N.; Habibi-Yangjeh, A.; Pirhashemi, M.; Vadivel, S.: Boosted visible-light photocatalytic performance of TiO_{2-x} decorated by BiOI and AgBr nanoparticles. J. Photochem. Photobiol. A Chem. **384**, 112066 (2019). https://doi.org/10.1016/j.jphotochem.2019.112066
10. Wang, P.; Zhou, T.; Wang, R.; Lim, T.-T.: Carbon-sensitized and nitrogen-doped TiO_2 for photocatalytic degradation of sulfanilamide under visible-light irradiation. Water Res. **45**, 5015–5026 (2011). https://doi.org/10.1016/j.watres.2011.07.002
11. Huang, H.; Song, Y.; Li, N.; Chen, D.; Xu, Q.; Li, H.; He, J.; Lu, J.: One-step in-situ preparation of N-doped TiO_2@C derived from Ti_3C_2 MXene for enhanced visible-light driven photodegradation. Appl. Catal. B **251**, 154–161 (2019). https://doi.org/10.1016/j.apcatb.2019.03.066
12. Khalyavka, T.; Bondarenko, M.; Shcherban, N.; Petrik, I.; Melnyk, A.: Effect of the C and S additives on structural, optical, and photocatalytic properties of TiO_2. Appl. Nanosci. **9**, 695–702 (2019). https://doi.org/10.1007/s13204-018-0838-1
13. Ren, W.; Ai, Z.; Jia, F.; Zhang, L.; Fan, X.; Zou, Z.: Low temperature preparation and visible light photocatalytic activity of mesoporous carbon-doped crystalline TiO_2. Appl. Catal. B **69**, 138–144 (2007). https://doi.org/10.1016/j.apcatb.2006.06.015
14. Matos, J.; García, A.; Zhao, L.; Titirici, M.M.: Solvothermal carbon-doped TiO_2 photocatalyst for the enhanced methylene blue degradation under visible light. Appl. Catal. A Gen. **390**, 175–182 (2010). https://doi.org/10.1016/j.apcata.2010.10.009
15. Alsaiari, M.: Biomass-derived active carbon (AC) modified TiO_2 photocatalyst for efficient photocatalytic reduction of chromium (VI) under visible light. Arab. J. Chem. **14**, 103258 (2021). https://doi.org/10.1016/j.arabjc.2021.103258
16. Liu, G.; Xia, H.; Niu, Y.; Zhao, X.; Zhang, G.; Song, L.; Chen, H.: Photocatalytic performance of doped TiO_2/AC coating and its UV stability research. Prog. Org. Coat. **148**, 105882 (2020). https://doi.org/10.1016/j.porgcoat.2020.105882
17. Jiang, Z.; Zhang, X.; Yuan, Z.; Chen, J.; Huang, B.; Dionysiou, D.D.; Yang, G.: Enhanced photocatalytic CO_2 reduction via the synergistic effect between Ag and activated carbon in TiO_2/AC-Ag ternary composite. Chem. Eng. J. **348**, 592–598 (2018). https://doi.org/10.1016/j.cej.2018.04.180
18. Ilyas, S.; Abdullah, B.; Tahir, D.: Enhancement of absorbing frequency and photo-catalytic performance by temperature treatment of composites Fe_3O_4-AC nanoparticle. Adv. Powder Technol. **31**, 905–913 (2020). https://doi.org/10.1016/j.apt.2019.11.007
19. Tahir, D.; Abdullah, B.; Ilyas, S.; Fahri, A.N.; Anugrah, M.A.; Kim, K.; Kang, H.J.: Decreasing charge recombination by magnetic trap of iron-carbon (Fe-AC) composite for enhanced photocatalytic performance. Surf. Interface Anal. **53**, 446–459 (2021). https://doi.org/10.1002/sia.6932
20. Lahrar, E.H.; Simon, P.; Merlet, C.: Carbon–carbon supercapacitors: beyond the average pore size or how electrolyte confinement and inaccessible pores affect the capacitance. J. Chem. Phys. **155**, 184703 (2021). https://doi.org/10.1063/5.0065150
21. Mo, Z.; Yang, W.; Gao, S.; Shang, J.K.; Ding, Y.; Sun, W.; Li, Q.: Efficient oxygen reduction reaction by a highly porous, nitrogen-doped carbon sphere electrocatalyst through space confinement effect in nanopores. J. Adv. Ceram. **10**, 714–728 (2021). https://doi.org/10.1007/s40145-021-0466-1
22. Li, R.; Yang, W.; Gao, S.; Shang, J.; Li, Q.: Hydrous cerium oxides coated glass fiber for efficient and long-lasting arsenic removal from drinking water. J. Adv. Ceram. **10**, 247–257 (2021). https://doi.org/10.1007/s40145-020-0435-0
23. Sadeghzadeh-Attar, A.: Photocatalytic degradation evaluation of N-Fe codoped aligned TiO_2 nanorods based on the effect of annealing temperature. J. Adv. Ceram. **9**, 107–122 (2020). https://doi.org/10.1007/s40145-019-0353-1
24. Eshaghi, A.; Moradi, H.: Optical and photocatalytic properties of the Fe-doped TiO_2 nanoparticles loaded on the activated carbon. Adv. Powder Technol. **29**, 1879–1885 (2018). https://doi.org/10.1016/j.apt.2018.04.026

25. Ilyas, S.; Heryanto, H.; Tahir, D.: Correlation between structural and optical properties of CuO/carbon nanoparticle in supports the photocatalytic performance and attenuate the electromagnetic wave. J. Environ. Chem. Eng. **9**, 104670 (2021). https://doi.org/10.1016/j.jece.2020.104670
26. Zhu, X.; Li, Q.; Fang, Y.; Liu, X.; Xiao, L.; Ai, X.; Yang, H.; Cao, Y.: Graphene-modified TiO_2 microspheres synthesized by a facile spray-drying route for enhanced sodium-ion storage. Part. Part. Syst. Charact. **33**, 545–552 (2016). https://doi.org/10.1002/ppsc.201500216
27. Brown, G.N.; Birks, J.W.; Koval, C.A.: Development and characterization of a titanium dioxide-based semiconductor photoelectrochemical detector. Anal. Chem. **64**, 427–434 (1992). https://doi.org/10.1021/ac00028a018
28. Abdullah, B.; Ilyas, S.; Tahir, D.: Nanocomposites Fe/activated carbon/PVA for microwave absorber: synthesis and characterization. J. Nanomater. **2018**, 9823263 (2018). https://doi.org/10.1155/2018/9823263
29. Heryanto, H.; Abdullah, B.; Tahir, D.: Analysis of structural properties of X-ray diffraction for composite copper-activated carbon by modified Williamson–Hall and size-strain plotting methods. J. Phys. Conf. Ser. **1080**, 012007 (2018). https://doi.org/10.1088/1742-6596/1080/1/012007
30. Rauf, N.; Ilyas, S.; Heryanto, H.; Rahmat, R.; Fahri, A.N.; Rahmi, M.H.; Tahir, D.: The correlation between structural and optical properties of zinc hydroxide nanoparticle in supports photocatalytic performance. Opt. Mater. (Amst.) **112**, 110780 (2021). https://doi.org/10.1016/j.optmat.2020.110780
31. Anugrahwidya, R.; Yudasari, N.; Tahir, D.: Optical and structural investigation of synthesis ZnO/Ag Nanoparticles prepared by laser ablation in liquid. Mater. Sci. Semicond. Process. **105**, 104712 (2020). https://doi.org/10.1016/j.mssp.2019.104712
32. Tahir, D.; Suarga; Sari, N.H.; Yulianti: Stopping powers and inelastic mean free path of 200eV–50keV electrons in polymer PMMA, PE, and PVC. Appl. Radiat. Isotopes **95**, 59–62 (2015). https://doi.org/10.1016/j.apradiso.2014.10.001
33. Tahir, D.; Heryanto, H.; Ilyas, S.; Fahri, A.N.; Rahmat, R.; Rahmi, M.H.; Taryana, Y.; Sukaryo, S.G.: Excellent electromagnetic wave absorption of Co/Fe_2O_3 composites by additional activated carbon for tuning the optical and the magnetic properties. J. Alloys Compd. **864**, 158780 (2021). https://doi.org/10.1016/j.jallcom.2021.158780
34. Ulum, B.; Ilyas, S.; Fahri, A.N.; Mutmainna, I.; Anugrah, M.A.; Yudasari, N.; Demmalino, E.B.; Tahir, D.: Composite carbon-lignin/zinc oxide nanocrystalline ball-like hexagonal mediated from *Jatropha curcas* L leaf as photocatalyst for industrial dye degradation. J. Inorg. Organomet. Polym. Mater. **30**, 4905–4916 (2020). https://doi.org/10.1007/s10904-020-01631-5
35. Pambudi, A.B.; Kurniawati, R.; Iryani, A.; Hartanto, D.: Effect of calcination temperature in the synthesis of carbon doped TiO_2 without external carbon source. AIP Conf. Proc. **2049**, 020074 (2018). https://doi.org/10.1063/1.5082479
36. Suganthi, N.; Thangavel, S.; Kannan, K.: Hibiscus subdariffa leaf extract mediated 2-D fern-like ZnO/TiO_2 hierarchical nanoleaf for photocatalytic degradation. FlatChem **24**, 100197 (2020). https://doi.org/10.1016/j.flatc.2020.100197
37. Bagheri, S.; Shameli, K.; Abd Hamid, S.B.: Synthesis and characterization of anatase titanium dioxide nanoparticles using egg white solution via sol–gel method. J. Chem. **2013**, 848205 (2013). https://doi.org/10.1155/2013/848205
38. Indira, K.; KamachiMudali, U.; Rajendran, N.: In vitro bioactivity and corrosion resistance of Zr incorporated TiO_2 nanotube arrays for orthopaedic applications. Appl. Surf. Sci. **316**, 264–275 (2014). https://doi.org/10.1016/j.apsusc.2014.08.001
39. Rauf, M.; Ashraf, S.: Fundamental principles and application of heterogeneous photocatalytic degradation of dyes in solution. Chem. Eng. J. **151**, 10–18 (2009). https://doi.org/10.1016/j.cej.2009.02.026
40. Rizkayanti, Y.; Yusuf, Y.: Optimization of the temperature synthesis of hydroxyapatite from Indonesian crab shells. Int. J. Nanoelectron. Mater. **12**, 85–92 (2019)
41. Fakhrul Ridhwan Samsudin, M.; Sufian, S.; Bashiri, R.; Muti Mohamed, N.; Tau Siang, L.; Mahirah Ramli, R.: Optimization of photodegradation of methylene blue over modified TiO_2/$BiVO_4$ photocatalysts: effects of total TiO_2 loading and different type of co-catalyst. Mater. Today Proc. **5**, 21710–21717 (2018). https://doi.org/10.1016/j.matpr.2018.07.023
42. Yu, H.; Zhao, Y.; Zhou, C.; Shang, L.; Peng, Y.; Cao, Y.; Wu, L.-Z.; Tung, C.-H.; Zhang, T.: Carbon quantum dots/TiO_2 composites for efficient photocatalytic hydrogen evolution. J. Mater. Chem. A Mater. **2**, 3344–3351 (2014). https://doi.org/10.1039/C3TA14108J
43. Yang, Y.; Gao, P.; Wang, Y.; Sha, L.; Ren, X.; Zhang, J.; Chen, Y.; Wu, T.; Yang, P.; Li, X.: A direct charger transfer from interface to surface for the highly efficient spatial separation of electrons and holes: the construction of Ti–C bonded interfaces in TiO_2-C composite as a touchstone for photocatalytic water splitting. Nano Energy **33**, 29–36 (2017). https://doi.org/10.1016/j.nanoen.2017.01.030
44. Munguti, L.; Dejene, F.: Influence of annealing temperature on structural, optical and photocatalytic properties of ZnO–TiO_2 composites for application in dye removal in water. Nano-Struct. Nano-Obj. **24**, 100594 (2020). https://doi.org/10.1016/j.nanoso.2020.100594
45. Nemoto, S.; Ueno, T.; Watthanaphanit, A.; Hieda, J.; Saito, N.: Crystallinity and surface state of cellulose in wet ball-milling process: ARTICLE. J. Appl. Polym. Sci. (2017). https://doi.org/10.1002/app.44903
46. Xiao, Y.; Wang, Y.; Xiao, M.; Liu, C.; Hou, S.; Ge, J.; Xing, W.: Regulating the pore structure and oxygen vacancies of cobaltosic oxide hollow dodecahedra for an enhanced oxygen evolution reaction. NPG Asia Mater. **12**, 73 (2020). https://doi.org/10.1038/s41427-020-00255-y
47. Zhang, J.; Li, J.: The oxygen vacancy defect of ZnO/NiO nanomaterials improves photocatalytic performance and ammonia sensing performance. Nanomaterials **12**, 433 (2022). https://doi.org/10.3390/nano12030433
48. Yakovenko, O.; Matzui, L.; Vovchenko, L.; Viktor, O.; Zagorodnii, V.; Trukhanov, S.; Trukhanov, A.: Electromagnetic properties of carbon nanotube/$BaFe_{12-x}Ga_xO_{19}$/epoxy composites with random and oriented filler distributions. Nanomaterials (Basel) **11**, 2873 (2021). https://doi.org/10.3390/nano11112873
49. Kozlovskiy, A.L.; Zdorovets, M.: v: Study of hydrogenation processes in radiation-resistant nitride ceramics. J. Mater. Sci. Mater. Electron. **31**, 11227–11237 (2020). https://doi.org/10.1007/s10854-020-03671-6
50. Kozlovskiy, A.; Egizbek, K.; Zdorovets, M.V.; Ibragimova, M.; Shumskaya, A.; Rogachev, A.A.; Ignatovich, Z.V.; Kadyrzhanov, K.: Evaluation of the efficiency of detection and capture of manganese in aqueous solutions of feceox nanocomposites doped with nb2o5. Sensors **20**, 4851 (2020)
51. Wang, B.; Yang, S.-Z.; Chen, H.; Gao, Q.; Weng, Y.-X.; Zhu, W.; Liu, G.; Zhang, Y.; Ye, Y.; Zhu, H.; Li, H.; Xia, J.: Revealing the role of oxygen vacancies in bimetallic $PbBiO_2Br$ atomic layers for boosting photocatalytic CO_2 conversion. Appl. Catal. B **277**, 119170 (2020). https://doi.org/10.1016/j.apcatb.2020.119170
52. Martins, A.C.; Cazetta, A.L.; Pezoti, O.; Souza, J.R.B.; Zhang, T.; Pilau, E.J.; Asefa, T.; Almeida, V.C.: Sol–gel synthesis of new TiO_2/activated carbon photocatalyst and its application for degradation of tetracycline. Ceram. Int. **43**, 4411–4418 (2017). https://doi.org/10.1016/j.ceramint.2016.12.088
53. Gao, X.; Ren, P.-G.; Wang, J.; Ren, F.; Dai, Z.; Jin, Y.-L.: Fabrication of visible-light responsive TiO_2@C photocatalyst with

an ultra-thin carbon layer to efficiently degrade organic pollutants. Appl. Surf. Sci. **532**, 147482 (2020). https://doi.org/10.1016/j.apsusc.2020.147482
54. Ji, L.; Zhang, Y.; Miao, S.; Gong, M.; Liu, X.: In situ synthesis of carbon doped TiO_2 nanotubes with an enhanced photocatalytic performance under UV and visible light. Carbon N Y **125**, 544–550 (2017). https://doi.org/10.1016/j.carbon.2017.09.094
55. Xin, Z.; Zhao, X.; Ji, H.; Ma, T.; Li, H.; Zhong, S.; Shen, Z.: Amorphous carbon-linked TiO_2/carbon nanotube film composite with enhanced photocatalytic performance: the effect of interface contact and hydrophilicity. Chin. Chem. Lett. **32**, 2151–2154 (2021). https://doi.org/10.1016/j.cclet.2020.11.054
56. Kamil, A.M.; Mohammed, H.T.; Balakit, A.A.; Hussein, F.H.; Bahnemann, D.W.; El-Hiti, G.A.: Synthesis, characterization and photocatalytic activity of carbon nanotube/titanium dioxide nanocomposites. Arab. J. Sci. Eng. **43**, 199–210 (2018). https://doi.org/10.1007/s13369-017-2861-z
57. Askari, M.B.; Tavakoli Banizi, Z.; Seifi, M.; Bagheri Dehaghi, S.; Veisi, P.: Synthesis of TiO_2 nanoparticles and decorated multiwall carbon nanotube (MWCNT) with anatase TiO_2 nanoparticles and study of optical properties and structural characterization of TiO_2/MWCNT nanocomposite. Optik (Stuttg) **149**, 447–454 (2017). https://doi.org/10.1016/j.ijleo.2017.09.078
58. Cheng, L.; Sun, L.; Xue, W.; Zeng, Z.; Li, S.: Adsorption equilibrium and kinetics of Pb(II) from aqueous solution by modified walnut shell. Environ. Prog. Sustain. Energy **35**, 1724–1731 (2016). https://doi.org/10.1002/ep.12424
59. de Benedetto, C.; Macario, A.; Siciliano, C.; Nagy, J.B.; de Luca, P.: Adsorption of reactive blue 116 dye and reactive yellow 81 dye from aqueous solutions by multi-walled carbon nanotubes. Materials **13**, 1–14 (2020). https://doi.org/10.3390/ma13122757
60. Fernandez, M.E.; Ledesma, B.; Román, S.; Bonelli, P.R.; Cukierman, A.L.: Development and characterization of activated hydrochars from orange peels as potential adsorbents for emerging organic contaminants. Bioresour. Technol. **183**, 221–228 (2015). https://doi.org/10.1016/j.biortech.2015.02.035
61. Selvi, N.; Sankar, S.; Dinakaran, K.: Effect of shell ZnO on the structure and optical property of TiO_2 core@shell hybrid nanoparticles. J. Mater. Sci. Mater. Electron. **26**, 2271–2277 (2015). https://doi.org/10.1007/s10854-015-2680-5
62. Xu, F.; Chen, J.; Kalytchuk, S.; Chu, L.; Shao, Y.; Kong, D.; Chu, K.-H.; Sit, P.H.-L.; Teoh, W.Y.: Supported gold clusters as effective and reusable photocatalysts for the abatement of endocrine-disrupting chemicals under visible light. J. Catal. **354**, 1–12 (2017). https://doi.org/10.1016/j.jcat.2017.07.027